Optimal Torque-Vectoring Control Strategy for Energy Efficiency and Vehicle Dynamic Improvement of Battery Electric Vehicles with Multiple Motors

2023-01-0563 Published 11 Apr 2023

Optimal Torque-Vectoring Control Strategy for Energy Efficiency and Vehicle Dynamic Improvement of Battery Electric Vehicles with Multiple Motors

Raffaele Manca, Luis MIguel Castellanos Molina, Shailesh Hegde, Andrea Tonoli, and Nicola Amati
Politecnico di Torino

Luigi Pazienza Silk Sports Car Company Srl

Citation: Manca, R., Castellanos Molina, L.M., Hegde, S., Tonoli, A. et al., "Optimal Torque-Vectoring Control Strategy for Energy Efficiency and Vehicle Dynamic Improvement of Battery Electric Vehicles with Multiple Motors," SAE Technical Paper 2023-01-0563, 2023, doi:10.4271/2023-01-0563.

Abstract

Electric vehicles comprising multiple motors allow the individual wheel torque allocation, i.e. torque-vectoring. Powertrain configurations with multiple motors provide additional degree of freedom to improve system level efficiencies while ensuring handling performances and active safety. However, most of the works available on this topic do not simultaneously optimize both vehicle dynamic performance and energy efficiency while considering the real-time implementability of the controller. In this work, a new and systematic approach in designing, modeling, and simulating the main layers of a torque-vectoring control framework is introduced. The high level control combines the actions of an adaptive Linear Quadratic Regulator (A-LQR) and of a feedforward controller, to shape the steady-state and transient vehicle response by generating the reference yaw moment. A novel energy efficient torque allocation method is proposed as a low level controller. The torque is allocated on each wheel by solving a quadratic programming problem. The latter is solved in real-time to guarantee the desired yaw moment and the requested driver power demand while minimizing the system losses. The objective function of the quadratic problem accounts for the efficiency map of the electric machine as well as the dissipations due to tire slip phenomena. The torque-vectoring is evaluated in a co-simulation environment. Matlab/Simulink is used for the control strategy and VI-CarRealTime for the vehicle model and driver. The vehicle model represents a high performance pure electric SUV with four e-motors. The performance of the proposed controller is assessed using open loop maneuvers and in closed loop track lap scenarios. The results demonstrate that the proposed controller enhances the vehicle's performance in terms of handling. Additionally, a significant improvement in energy saving in a wide range of lateral acceleration conditions is: presented. Moreover, the control strategy is validated using rapid control prototyping, thus guaranteeing a deterministic real-time implementation.

Introduction

Vehicle electrification has opened a wide range of opportunities regarding powertrain layouts and exploitable capabilities. Multiple motors architectures, which may have an onboard (the motors are part of the sprung mass), or an in-wheel layout (the motor is part of the unsprung mass) [1]. Multiple motors layout provides an additional degree of freedom to improve handling performances, active safety and system level efficiencies by leveraging electric machine control [2]. In this vehicle's layout, the powertrain acts as a chassis actuator, as it allows to control the wheel torque distribution [3], i.e., the torque-vectoring (TV). Comprehensive literature is available on TV systems, describing the active safety and handling benefits of applying a direct yaw moment through a suitable left-to-right wheel torque distribution [1, 2, 3, 4, 5, 6, 7]. In vehicle architectures with four e-motors, the TV system results are more effective due to the actuation redundancy which allows having a large set of possibilities to distribute the torque between the electric machines, paving the way to optimum control allocation strategies [8]. Thus, besides the improvement in vehicle dynamic performances, TV systems can be optimized for minimizing vehicles' power losses, reducing the energy consumption in straight line and cornering scenarios [9].

In the majority of the works proposed on the topic, the typical TV control framework is composed of three main layers [10]:

(i) a reference generator layer computes a target yaw rate $\dot{\psi}_{ref}$ and sideslip angle β_{ref} based on the driver inputs (steering wheel angle δ_{SW}, throttle, and brake pedal position) and on the estimated vehicle states (longitudinal and lateral acceleration a_x and a_y, vehicle speed V_x). (ii) A high-level TV control

layer generating the suitable yaw moment target M_z to achieve the desired reference behavior. Finally, in the torque allocation layer, (iii) the individual reference torque T_i to each electric motor is computed. The aim is to guarantee the overall traction torque T_{req} required by the driver and to achieve the yaw moment M_z defined in layer 2.

In the available literature, the reference value of the yaw rate defined in layer 1, generally has the aim to shape the understeering response [11] and to guarantee the vehicle's stability [12]. A wide variety of control formulations has been proposed for the high level TV control (layer 2). Feedback controllers based on Proportional Integral Derivative (PID) controllers [13], or model-based Linear Quadratic Regulator (LQR) [1], show good tracking results but often provide a synthetic driving feeling [2]. On the other hand, open loop feedforward controllers cannot guarantee the vehicle's stability, especially in conditions near the limits of handling. More sophisticated control techniques such as nonlinear model predictive control (NMPC) [9] or sliding mode controller (SMC) [14] are discussed in the literature, demonstrating good control performance, but they require high computation effort. Finally, the torque allocation algorithm, responsible for providing the reference torque value to each individual wheel, strictly depends on the application's powertrain topology, exploiting different torque allocation problem formulations.

Most of the cited TV applications focus on enhancing vehicle dynamics and active safety performance. In the context of electric vehicles, energy efficiency evaluation is a critical aspect to account in TV control framework design and implementation. Thus, several examples of energy-efficient TV are available in the literature [2, 3, 8, 9, 10]. To this end, the most used approach consists in reducing the different contributions of power losses. [15] proposes a detailed analysis for determining different contributions of power losses during torque-vectoring applications. The opportunity to minimize losses arises due to dissipations in powertrain and tire slip. The majority of the works on the topic implement the reduction of power losses through an energy-efficient torque allocation algorithm. In [2], a rule-based heuristic-optimized torque distribution layer is designed and validated. Other approaches are based on optimization problems for energy-efficient torque allocation. [16] solves an off-line optimization problem using a quasistatic nonlinear vehicle model, storing the routines in look-up tables. [17] determines a rule-based algorithm for combining energy-efficient reference yaw rate generation and torque distribution. With the increased available computational power of automotive hardware, some examples of real-time optimization routines are present in the literature. In [18], an integrated chassis control (ICC) for optimized tire force coordination is developed, while [9] enhances the energy efficiency in TV operation by exploiting nonlinear model predictive control.

In the sight of the aforementioned state-of-the-art analysis, it emerges that there is still a research gap in TV approaches that optimize in real-time the vehicle dynamic performance and the power efficiency at system level, while taking into account the real-time implementability of the controller and the computational efficiency.

Hence, to address the mentioned open point, an optimal torque-vectoring controller is proposed. It combines the action of a model-based feedforward to enhance the agility of the vehicle in transient maneuvers, with the action of an adaptive linear quadratic regulator to shape the understeering response of the vehicle and to guarantee the stability limits. The energy efficiency is considered in the torque allocation layer by proposing a novel approach in torque distribution. An optimization problem for torque allocation is presented, it is based on a quadratic objective function with real time constraints. The optimization problem is solved real-time to minimize the main sources of power losses integrating the constraints due to tire slip and e-motors capabilities.

The paper is structured as follows. The methodology is described in the section "torque-vectoring control". In the subsection "vehicle model" the model formulation is addressed, while the LQR and the feedforward control contributions are presented in the sections "adaptive LQR controller" and "model-based feedforward controller" respectively. The energy efficient torque allocation strategy is analyzed in the sections: "sources of power losses" and "torque allocation optimization problem". In the paragraph "results", the performance of the controller is assessed through model in the loop (MIL) approach with both open loop and closed loop maneuvers. The latter are evaluated in "processor in the loop" (PIL) setup, to validate the real time capability of the algorithm. Finally, the "conclusions" of the work are reported.

Torque-Vectoring Control

The overall control architecture of the proposed controller is reported in Figure 1. The inputs provided by the driver are the steering wheel angle δ_{SW} and the throttle and brake pedal position signals. The throttle/brake pedal position is used to compute the total traction force and consequently the total torque request T_{req}. The total torque request in traction is computed with throttle position and is constrained with the total available torque in e-motors for given rotational speed. The look-up table embedded in the controller sets the total available torque for traction. In recuperation, the brake pedal position is used to compute the brake torque demand to each wheel. Taking into account the regenerative braking capability of each electric machine at the operating point, the brake torque is split between the e-motors and mechanical brakes. The former is combined with the traction torque to compute the overall T_{req}.

The steering wheel angle is associated with the governing equations of the reference generator layer and the internal vehicle model of the TV controller. The corrective yaw moment M_z is provided by the sum of the contribution from the adaptive LQR and feedforward control action.

Finally, the aim of the torque allocation layer is to generate a torque reference to each wheel, trying to satisfy both the overall traction requirement T_{req} and the corrective yaw moment M_z while accounting for the limitation in actuation due to the e-motors' characteristics. This layer introduced a first step of anti-slip function, and moreover, it optimizes each e-motor torque reference by minimizing the power losses.

In the following subsections, each subsystem of the TV control pipeline is described in detail.

FIGURE 1 Torque-vectoring control architecture block scheme.

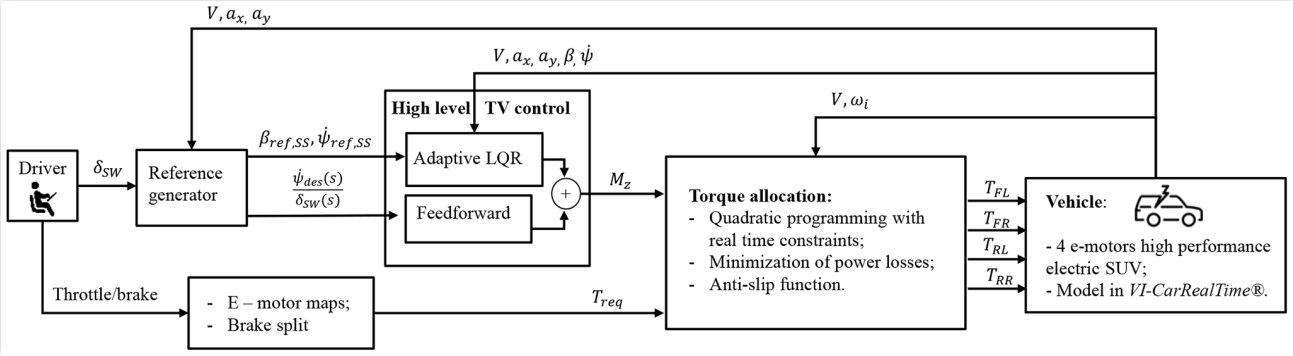

Vehicle Model Formulation

The case study used for the development of the discussed controller is a four wheel drive sport utility battery electric vehicle. It features four electric on-board motors, coupled to the wheels through a fixed transmission ratio. The vehicle is equipped with double wishbone and multilink suspension scheme at the front and the rear axle respectively. The main parameters of the vehicle are reported in Table 1.

The lateral dynamics of the vehicle is modeled by referring to the nonlinear single track model [6, 19] reported in Figure 2 based on the lateral force and yaw moment balance equations.

$$\begin{cases} mv_x\left(\dot{\beta}+\dot{\psi}\right)=F_{yF}+F_{yR} \\ J_z\ddot{\psi}=F_{yF}l_F-F_{yR}l_R+M_z \end{cases} \quad (1)$$

Where the front and rear lateral forces (F_{yF},F_{yR}) are obtained from the tire characteristics according to the Pacejka formulation [20].

$$F_{y,ij}=D_{ij}\,sin\left\{C_{ij}\,arctan\left[B_{ij}\alpha_i\ldots-E_{ij}\left(B_{ij}\alpha_i-arctan\left(B_{ij}\alpha_i\right)\right)\right]\right\} \quad (2)$$

B_{ij}, C_{ij}, D_{ij} are parameters of the tires provided by the manufacturer referred to the i (front or rear), j (left or right) wheel. These parameters are a function of the wheel vertical tire load $F_{z,\,ij}$ and of the tire–road friction coefficient μ. The vertical forces are computed considering the load transfer for a rigid vehicle model as [7], as function of the c.o.g. longitudinal a_x and lateral a_y acceleration:

$$F_{z,ij}=m\left(\frac{l_{F/R}}{l}g\pm\frac{h_G}{l}a_x\right)\left(\frac{1}{2}\pm\frac{h_G a_y}{tw_{F/R}g}\right) \quad (3)$$

l is the wheelbase and g the gravitational constant. Thus the lateral force exerted by each tire is a non-linear function of the vertical load and the sideslip angle of the tire α_i. The sideslip angle at the front and rear tires are geometrically

FIGURE 2 Single track vehicle model.

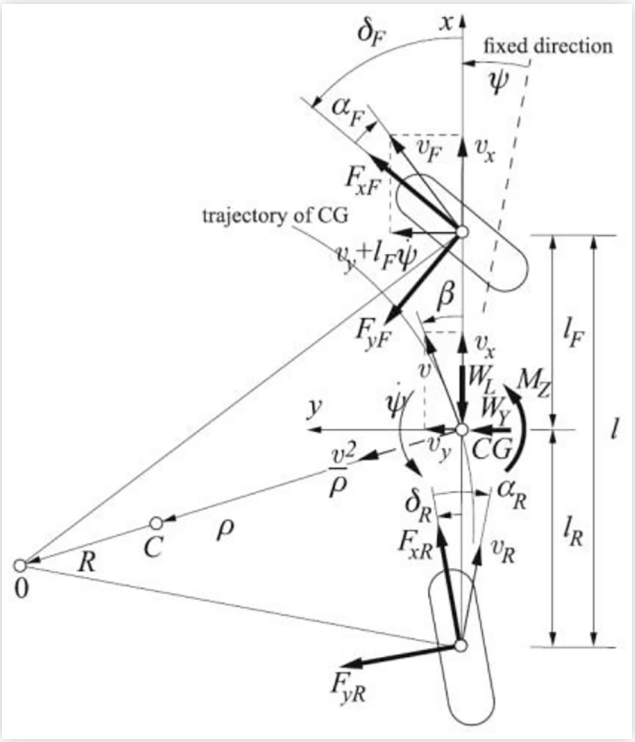

TABLE 1 Vehicle main parameters

Mass (m)	2100 kg
Yaw moment of inertia (J_z)	3300 kg m2
Distance of center of gravity (c.o.g.) from front axle (l_F)	1.48 m
Distance of center of gravity from rear axle (l_R)	1.48 m
Front and rear trackwidth ($tw_{F/R}$)	1.63 m
Height of c.o.g. (h_G)	0.64
Maximum rear e-motors power	300 kW
Maximum rear e-motors speed	25000 rpm
Maximum front e-motors power	150 kW
Maximum front e-motors speed	25000 rpm
Gear ratio e-motors to wheel (τ)	10:1
Tire	275/30R 21

obtained as a function of the longitudinal velocity v_x, the yaw rate $\dot{\psi}$, the steering angle δ_F, and the sideslip angle β.

$$\begin{cases} \alpha_F = \delta_F - \dfrac{l_F\dot{\psi}}{v_x} - \beta \\ \alpha_R = \dfrac{l_R\dot{\psi}}{v_x} - \beta \end{cases} \tag{4}$$

The equations (1)-(4) are used to model the vehicle's non-linear time domain lateral dynamic behavior. The vehicle sideslip angle and the yaw rate are the state variable $\boldsymbol{x}$ of the model. The input u is the corrective yaw moment. The steering angle δ_F is a disturbance to the model. The longitudinal velocity v_x, the longitudinal acceleration a_x, and the lateral acceleration a_y are considered as lumped time-varying parameters.

$$\begin{aligned} \dot{\boldsymbol{x}} &= f\left(\boldsymbol{x},\delta_F,v_x,a_x,a_y\right) + B_u u \\ \boldsymbol{x} &= \left[\beta,\dot{\psi}\right]^T, u = M_z, \delta_F = \delta_{SW}/15 \end{aligned} \tag{5}$$

In the powertrain subsystem, the characteristics of the four e-motors are modeled with two look-up tables of the maximum torque curves of the front and rear e-motors.

All the model's states and variables are assumed available from the chassis sensors, taken as feedback from the plant 14 d.o.f vehicle model developed in Vi Grade CarRealTime software. The development of estimation methods for non-directly measurable variables is out of the scope of the present work.

Reference Generator

In this subsystem, the reference values of the yaw rate and the vehicle sideslip angle are computed. These are used to shape the steady state vehicle response through the feedback control contribution. The reference transitory behavior for the feed-forward controller is described in the dedicated section "feedforward".

A tunable steady state yaw rate reference is reported for two selectable modes of the controller: "Sport" to enhance the vehicle sportivity and fun-to-drive behavior, and "Stability" for guaranteeing the safety in cornering. The sport formulation is function of the steering angle input and of the longitudinal speed, according to the single-track model.

$$\dot{\psi}_{ref,SS} = \begin{cases} \dot{\psi}_{max}\tanh\left(\dfrac{v_x\delta_F}{0.7l\left(1+K_{US}v_x^2\right)\dot{\psi}_{max}}\right), & Sport \\ \dot{\psi}_{max}\tanh\left(\dfrac{\psi}{\dot{\psi}_{max}}\right), & Stability \end{cases} \tag{6}$$

where K_{US} is the understeering coefficient. The yaw rate stability limit $\dot{\psi}_{max}$ is function of the friction coefficient μ and of the speed v_x as:

$$\dot{\psi}_{max} = \frac{\mu g}{v_x} \tag{7}$$

The reference sideslip angle is evaluated as:

$$\beta_{ref,SS} = \beta_{\max}\, tanh\left(\frac{\beta}{\beta_{max}}\right) \tag{8}$$

The sideslip limit β_{max} is given by the empirical formulation [6]:

$$\beta_{max} = \tan^{-1}\left(0.02\mu g\right) \tag{9}$$

Adaptive Linear Quadratic Regulator

The proposed LQR contribution aims to stabilize the open loop action of the feedforward controller and to shape the steady state response of the vehicle. The model is based on the single track formulation, including the tire non-linearities reported in equations (1)-(5).

Due to the non-linear nature of the problem, the system is linearized by exploiting a symbolic formulation of the Jacobian matrices. The Jacobian matrices, J_A, J_{BD} and J_{Bu}, are then updated each time-step with the current states and parameters.

$$\dot{\boldsymbol{x}} = J_A\boldsymbol{x} + J_{BD}\delta_F + J_{Bu}u \tag{10}$$

The control input u (the corrective yaw moment M_z) is computed minimizing the cost function:

$$J = \int_0^\infty \left(\boldsymbol{x}^T Q\boldsymbol{x} + uRu\right)dt \tag{11}$$

Where the weight matrix Q is:

$$Q = \begin{bmatrix} \dfrac{1}{\beta_{max}^2} & 0 \\ 0 & \dfrac{1}{\dot{\psi}_{max}^2} \end{bmatrix} \tag{12}$$

With the limit values of sideslip angle and yaw rate computed as in (7) and (9). The control effort matrix is computed as:

$$R = \frac{1}{M_{z,max}^2} \tag{13}$$

The maximum yaw moment $M_{z,\ max}$ is given by:

$$M_{z,max} = \frac{tw_F}{2}\left|F_{x,FR,max} - F_{x,FL,max}\right| + \frac{tw_R}{2}\left|F_{x,RR,max} - F_{x,RL,max}\right| \tag{14}$$

$F_{x,\ ij,\ max}$ is the maximum longitudinal force that the i, j wheel (front/rear, left/right) can exert. This force is determined according to the e-motor maximum torque available at the measured working speed and to the tire force to avoid slip for the vertical load of the wheel:

$$F_{x,ij,max} = \min\left(\frac{\tau \cdot T_{EM,max,\omega EM,ij}}{R_e}, F_{x,ij(\sigma=max,Fzij)} \right) \quad (15)$$

The longitudinal force exerted by the tires F_x, is function of the longitudinal slip ratio σ, derived from the Pacejka Magic Formula formulation [20], including the longitudinal tire parameters provided by the tire manufacturer. The effective rolling radius (R_e) is assumed to be equal to the loaded radius function of the tire's vertical load and the tire's vertical stiffness [19].

Hence, the control action of the LQR is:

$$M_{z,LQR} = \mathrm{K}_{LQR} \begin{pmatrix} \beta_{ref} - \beta \\ \dot{\psi}_{ref} - \dot{\psi} \end{pmatrix} \quad (16)$$

Model-Based Feedforward

The open loop contribution, provided by the feedforward controller, aims to enhance the vehicle's agility and responsiveness. The feedforward controller forces the vehicle to behave in a more agile manner. The LQR shapes the response in steady state conditions, while the feedforward is designed to provide a faster response in transient conditions.

The feedforward action is expressed in Laplace notation as follows:

$$FF(s) = \frac{M_{z,FF}(s)}{\delta_F(s)} = \frac{G_{des}(s) - G_{nom}(s)}{G_p(s)}$$
$$G_{des}(s) = \frac{\dot{\psi}_{des}(s)}{\delta_F(s)}, G_{nom}(s) = \frac{\dot{\psi}(s)}{\delta_F(s)}, G_p(s) = \frac{\dot{\psi}(s)}{M_{z,FF}(s)} \quad (17)$$

$G_{des}(s)$ is the front-end response of a vehicle with a reduced inertia moment ($0.75 \cdot J_z$). $G_{nom}(s)$ is the response of the actual vehicle, and $G_p(s)$ is the frequency response between the yaw rate generation to the yaw moment input. All above mentioned transfer functions are related to the non-linear single track model reported in the previous sections.

Similarly to the adaptive LQR approach, the feedforward is designed by linearizing the $FF(s)$ transfer function through symbolic Jacobian formulation. At each time step, the feedforward is updated to the current states and parameters generating the yaw moment response to the steering input.

Estimation of Power Losses

The power losses analyzed in this study are due to two main contributions. Firstly due to the dissipations in the powertrain and secondly due to losses at the tire ground contact caused by longitudinal and lateral slip. These losses are affected by the understeer characteristic of the vehicle, and also by the torque control and allocation strategy.

The power losses of the powertrain unit are a function of the e-motor's efficiency, transmission stages and inverter's characteristics. In this analysis, only the losses in the e-motors are considered. Hence, the power losses of each electric motor can be derived from the speed – torque – efficiency characteristic (Figure 3) as:

$$P_{loss,EM} = \begin{cases} P_{el.} - P_{mech.} = \dfrac{T\omega_{EM}}{\eta_{EM}} - T\omega_{EM}, \ Traction \\ P_{mech.} - P_{el.} = T\omega_{EM} - T\omega_{EM}\eta_{EM}, \ Braking \end{cases} \quad (18)$$

Where $P_{el.}$ and $P_{mech.}$ are the electric and mechanical power respectively. T is the torque of the motor, ω_{EM} is the rotational speed of the rotor and η_{EM} is the efficiency on the e-motor at the considered working point. In order to evaluate and minimize the powertrain losses in real-time, a quadratic formulation of the electric power $P_{el.}$ as function of the rotational speed ω_{EM} and torque T has been derived. This formulation is obtained by the second order polynomial fitting of the efficiency curves of Figure 3, by exploiting the Least-squares error method.

$$P_{el.est.} = a_1\omega_{EM}T + a_2\omega_{EM}^2T + a_3\omega_{EM}T^2 + a_4\omega_{EM} + a_5T \quad (19)$$

Both the front and rear e-motors curves has been fitted. The electrical power is estimated in both traction and braking operation to have a single polynomial equation of the electric power. The goodness of fit for the coefficients of rear motors a_{ir} is 97.38% whereas it is 96.51% for coefficients for the front e-motors a_{if}. In this way the e-motor's power losses can be formulated as function of the rotational speed (computed by the encoder sensors model) and by the torque, which

FIGURE 3 (a) Front e-motors efficiency map. (b) Rear e-motors efficiency map.

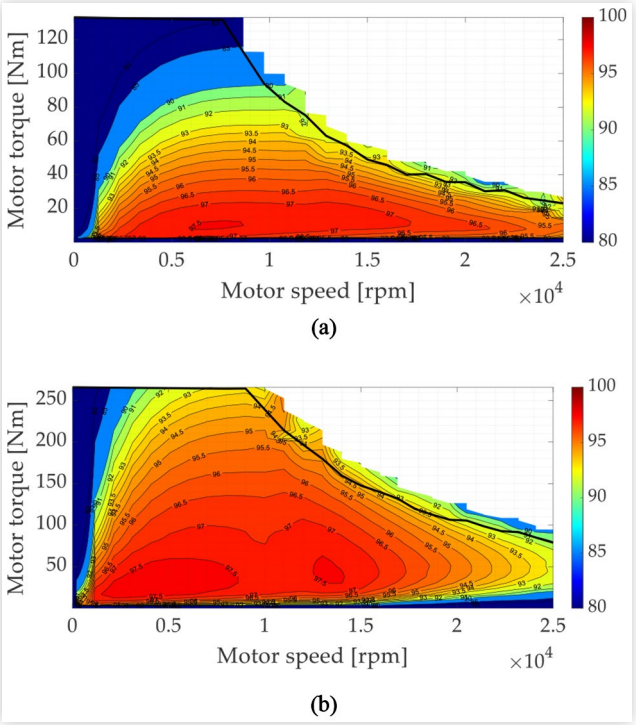

happens to be the control variable of the proposed torque allocation algorithm.

$$P_{loss.EM} = P_{el.est.} - P_{mech} = P_{el.est.} - T\,\omega_{EM} \tag{20}$$

Tire slip power losses are a function of the tire forces and of the slip velocity [15]. Therefore, the tire losses due to longitudinal slip are computed as:

$$P_{loss,tir.long} = F_x\left(v_{x,w} - \omega_w R_e\right) \approx \frac{\tau T}{R_e}\left(v_{x,w} - \omega_w R_e\right) \tag{21}$$

Where $v_{x,w}$ is the longitudinal tire frame component of the vehicle velocity vector at the center of the wheel. It can be geometrically computed for the *i*, *j* wheel as:

$$v_{x,ij} = v_x \cos\left(\delta_i - \beta\right) \pm \left((\dot{\psi} \cdot \sqrt{l_{F/R}^2 + \frac{tw_{F/R}}{2}}\right) \sin\left(\operatorname{atan}\left(\frac{tw_{F/R}}{2l_{F/R}}\right)\right) \tag{22}$$

Where ω_w is the wheel rotational speed. In order to have the longitudinal slip dissipation function of the torque delivered by the motor, the longitudinal force F_x is approximated as the product of the torque and the transmission ratio τ by the rolling radius R_e.

The power losses due to lateral tire slip, is defined as:

$$P_{loss,tir.lat.} = F_y\left(-v_x cos\beta \pm \frac{tw_{F/R}}{2}\right) \sin\delta_i \pm \left(v_x sin\beta + \dot{\psi}\, l_{F/R}\right) \cos\delta_i \tag{23}$$

The losses due to lateral slip are not a function of the torque, they are influenced by the understeer behavior and rather indirectly influenced by the torque allocation algorithm.

Torque Allocation Optimization Algorithm

In the torque allocation layer a suitable torque distribution is determined with the scope of guaranteeing both the overall traction torque required by the driver T_{req} and the reference corrective yaw moment M_z. In the following a quadratic programming problem with real time constraints, which accounts the energetic efficiency at vehicle level is proposed.

According to the control goals, the optimization problem is designed to minimize the following quadratic cost function:

$$\min\left(\frac{1}{2}\boldsymbol{x}^T H \boldsymbol{x} + \boldsymbol{f}^T \boldsymbol{x}\right) \tag{24}$$

Subject to:

$$\begin{cases} A_{eq}\boldsymbol{x} = \boldsymbol{b_{eq}} \\ A\boldsymbol{x} \le \boldsymbol{b} \\ \boldsymbol{lb} \le \boldsymbol{x} \le \boldsymbol{ub} \end{cases} \tag{25}$$

Where H is the Hessian matrix, containing the quadratic terms of the problem, and the vector $\boldsymbol{f}$ contains the linear terms.

The vector $\boldsymbol{x} = [T_{FL}, T_{FR}, T_{RL}, T_{RR}, Sl_{Treq}, Sl_{Mz}]^T$ is the unknown torques control vector. It contains the four motor torques (*FL* stands for front-left, *RR* stands for rear-right) and the two slack variables related to the overall torque (Sl_{Treq}) and yaw moment request (Sl_{Mz}) respectively. The slack variables are included in the problem to avoid infeasibility issues by transforming equality constraints into inequality [21]. The slack variables' weights can be tuned to prioritize the traction request or the yaw moment generation when the actuation limits are reached.

The system is constrained with equality to guarantee the following relations:

$$\begin{cases} T_{FL} + T_{FR} + T_{RL} + T_{RR} + Sl_{Treq,} = T_{Req,} \\ \tau\left[tw_F\left(\frac{T_{FR}}{R_{e,FR}} - \frac{T_{FL}}{R_{e,FL}}\right) + tw_R\left(\frac{T_{RR}}{R_{e,RR}} - \frac{T_{RR}}{R_{e,RR}}\right)\right] + Sl_{Mz} = M_z \end{cases} \tag{26}$$

Hence, $\boldsymbol{b_{eq}} = [T_{Req,} M_z]^T$; and

$$A_{eq} = \begin{bmatrix} 111110 \\ \frac{\tau \cdot tw_f}{R_{e,FL}} \frac{\tau \cdot tw_f}{R_{e,FR}} \frac{\tau \cdot tw_f}{R_{e,RL}} \frac{\tau \cdot tw_f}{R_{e,RR}} 01 \end{bmatrix}.$$

The first inequality constraint ($A\boldsymbol{x} \le \boldsymbol{b}$) is used to guarantee the sign consistency between the total torque request and the total torque applied, and between the yaw moment request and yaw moment applied.

The solutions are bounded of the vectors ***lb*** and ***ub*** considering the maximum regenerative and deliverable torque, by each e-motor at the instantaneous speed, and the maximum and minimum torque to avoid slip, similarly to Equation 15.

$$\boldsymbol{lb} = \left[\max\left(-k_{reg} Tmax_{EM,ij}, \frac{R_{e,ij} F_{xij(\sigma=min,Fzij)}}{\tau}\right), \ldots\right]^T$$
$$\boldsymbol{ub} = \left[\min\left(Tmax_{EM,ij}, \frac{R_{e,ij} F_{xij(\sigma=max,Fzij)}}{\tau}\right), \ldots\right]^T \tag{27}$$

With k_{reg} as the desired regeneration factor.

The objective function of the proposed problem has three terms to minimize:

$$\mathrm{J} = k_1 P_{loss.EM} + k_2 P_{loss,tir.long} + k_3\left(1 - \frac{F_{z,F/R}}{F_{z,TOT}}\right)\boldsymbol{x} \tag{28}$$

The first two terms represent the dissipations due the e-motors and to the longitudinal slip as function of the torques, derived in Equations (20) and (21) respectively. The aim of the last term is to make the torque distribution proportional to the longitudinal load transfer according to Equation 3. The three weights k_1, k_2, k_3 can be tuned for the desired design objective.

The objective function has to be rewritten in the standard quadratic programming formulation of Equation 25. H is a 6x6 diagonal matrix including the terms multiplying the torques quadratically and the weights assigned to the slack

variables. In the following results the slack variables have been tuned to prioritize the total traction torque request. The terms of Equations (19) - (21) multiplying linearly the torques, and term accounting the load transfer, are included in the 6x1vector ***f***.

It should be noted that the Hessian matrix H is positive definite. As a result, this minimization problem is convex [21]. This ensures that there is an unique solution. It is possible to calculate this solution using the closed-form solution or numerical methods that entail an iterative process[22]. The proposed constrained optimization problem is solved using the active set algorithm [23].

Results

In the following sections, the performance of the proposed torque-vectoring controller are evaluated. The controller is validated through model in the loop (MIL) and processor in the loop (PIL) approaches. For the former, the TV is co-simulated in Matlab-Simulink environment, where the controller is developed. The reference torques signals are provided to the vehicle plant, modeled in Vi-Grade CarRealTime. The 14 d.o.f. CarRealTime multibody vehicle model includes the characteristics of the e-motors and the performances of the tires through the .tir files. The feedback signals needed by the controller are directly taken from the sensor models in the CarRealTime plant. Open loop and closed loop maneuvers are performed in MIL set-up.

The controller is then validated by deploying it on a rapid prototyping control unit, the Speedgoat Baseline real-time target machine. In this set-up, the closed loop maneuvers are performed, by exploiting the driver modeled in CarRealTime on a race track scenario.

Open-Loop Performance Assessment

Open loop maneuvers allow the objective assessment of the vehicle response, decoupling the influence of the driver. In order to have a complete evaluation in all the lateral dynamic conditions two standard open loop maneuvers are performed:

- Slow ramp steer maneuver (SRS);
- Sine sweep with increasing frequency maneuver (SSI).

The SRS is carried out at the constant speed of 100 km/h. The steering wheel angle δ_{SW} is increased from 0 to 180 deg with a slope of 1 deg/s. The aim of the SRS maneuver is to characterize the steady state cornering behavior of the vehicle in the whole range of lateral acceleration up to the limits of adherence of the tires. The plot of the steering angle δ_{SW} as function of the lateral acceleration a_y allows to evaluate vehicle's understeer behavior, while the plot of the side slip angle β as a function of a_y can be used to assess the performance in terms of stability [24].

In Figure 4 the results of the SRS maneuver in MIL set-up for the case study vehicle, are reported. The test has been

FIGURE 4 Slow ramp steer (SRS) 100 km/h maneuver. (a), (b) Dry road, μ = 1. (c), (d) Wet road, μ = 0.4. Black dashed line = passive vehicle. Blue continuous line = TV "sport" tuning. Orange continuous line = TV "stability" tuning. (a), (c) Understeering curves. (b), (d) Sideslip angle curves.

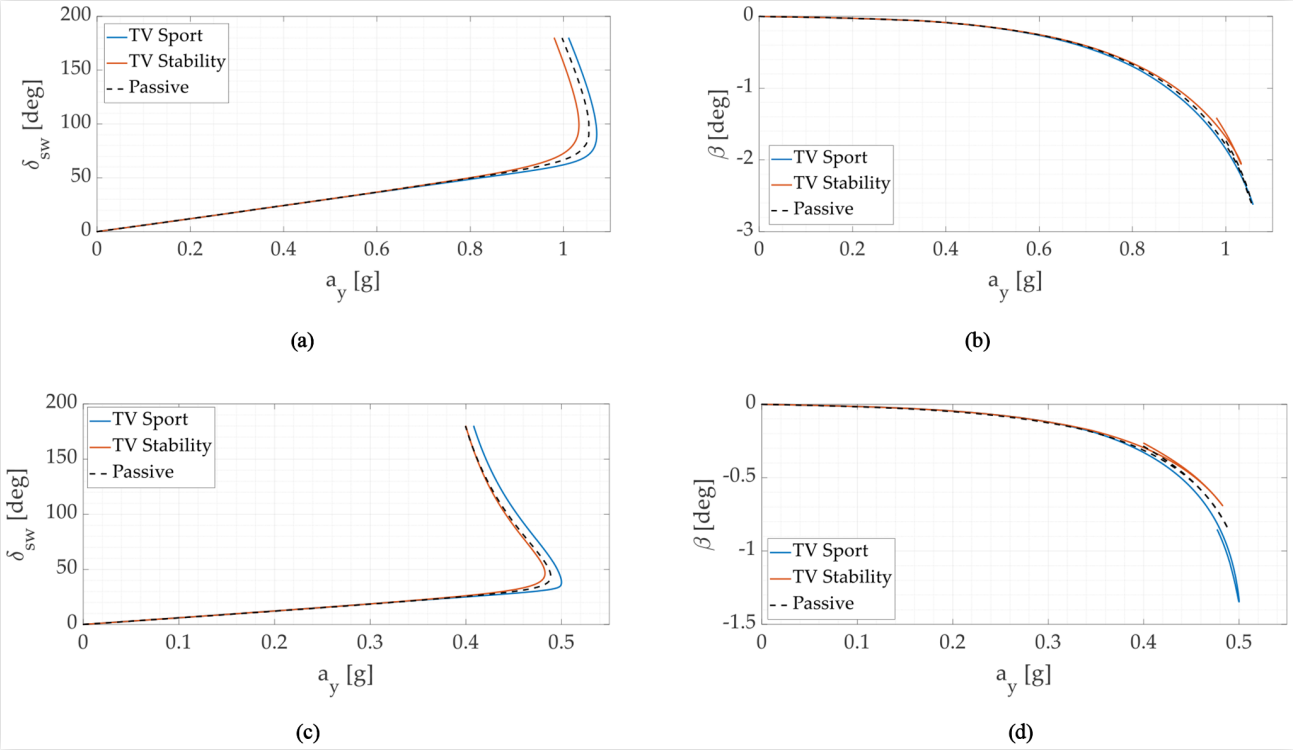

performed in dry asphalt condition (μ = 1), Figure 4 (a) and (b), and in low adherence, wet asphalt conditions ((μ = 0.4), Figure 4 (c) and (d)). For all the analysis the trend of the passive vehicle (dashed black line) is compared with the behavior of the vehicle with torque vectoring controller. In the TV controller, results for two different tunable modes are reported: the TV "sport" (blue line) and the TV "stability" (orange line), as defined in Equation 6.

The understeering curve is shown in Figure 4 (a), it can be seen that the TV sport allow to increase the maximum lateral acceleration $a_{y,\,max}$ 3% with respect to the passive vehicle. The TV sport mode, reduces the overall understeering tendency; this is more evident when the vehicle is approaching the limits of stability. Moreover, the steering wheel gradient in linear region, i.e. the slope of the understeering curve, ($g\delta_{lin}\big|_{ay=0.4\,g} = \frac{\partial \delta_{SW}}{\partial a_y}$) at 0.4g is same as of the passive vehicle. Instead, the slope of the understeering curve measured at the 85 % of $a_{y,\,max}$ ($g\delta|_{85\,\%\,ay,\,max}$) is reduced by 3.2 %. On the other hand, the "stability" mode of the controller enhances a more safer steady state behavior. The stability mode reduces the maximum acceleration ($a_{y,\,max}$) by 2 % and increases the understeering gradient by 1 %. The performance improvement in "stability" mode of TV controller, is shown in Figure 4 (b). The maximum sideslip angle β_{max}, is reduced by 15%, while its performance is unaffected by the sport mode. The stability mode TV controller improves the rear end stability of the vehicle, thus low sideslip angle is generated for the same lateral acceleration. The rear end stability improvement is evaluated with the slope of the sideslip angle curve: in linear conditions $g\beta_{lin}\big|_{ay=0.4\,g} = \frac{\partial \beta}{\partial a_y}$ is reduced by 1 %, while in the non-linear region $g\beta\big|_{85\%ay,max} = \frac{\partial \beta}{\partial a_y}$ is reduced of the 11 %. The ratio between the sideslip angle gradient in the non-linear region and in the linear region $\left(g\beta_{SO} = \frac{g\beta\big|_{85\%ay,max}}{g\beta_{lin}\big|_{ay=0.4\,g}}\right)$ is an indicator to evaluate the easiness to control the vehicle approaching the limits of stability [3]. $g\beta_{SO}$ is improved by 10 % for the "stability" mode and worsened by 5 % for the "sport" mode, in comparison to the passive vehicle. Also, similar improvement in performance holds true in low adherence conditions. Figure 4 (c) confirms how the two proposed versions of TV controller shapes the understeering curve even in wet road condition. Figure (d) highlight the stability performance improvement at limits of adherence.

In the SRS maneuver, the main contributors of power losses are calculated in post processing. In Figure 5 the main power losses are reported, according to Equations (18) - (23). The main losses contributions are provided by the dissipations due to tire slip (the 31 % of the total losses from the longitudinal, and the 61 % from the lateral). The developed controller ensures a reduction of the e-motor's dissipations, hence, the e-motors operates in high efficiency regions. The optimal torque allocation algorithm lead to the 53 % of longitudinal slip losses reduction. The mitigation of side slip losses are due to the improved understeering response of the TV controlled vehicle. Finally the torque-vectoring lead to the 2.9 % reduction of the overall energy consumption (measured at the DC bus) during the 180 s maneuver.

FIGURE 5 Mean Power losses in SRS 100 km/h (dry) maneuver.

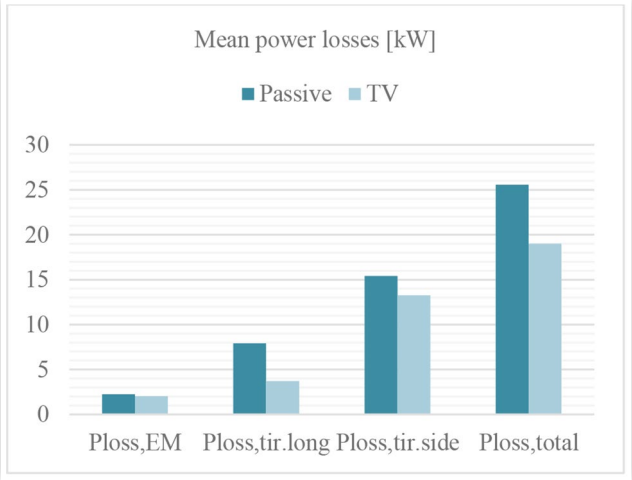

The sine sweep steering maneuver consists in providing a sinusoidal steering input with a frequency increasing from 0 to 10 Hz. The δ_{SW} amplitude is given by the steering angle value at which a lateral acceleration $a_y = 4\ m/s^2$ occurs in the stationary SRS test (Figure 4) [25]. The SSI is performed to assess the transient steering response of the vehicle. The transfer functions between the δ_{SW} input and the measured yaw rate $\dot{\psi}$ output (Figure 6) is used to evaluate the vehicle's agility. The transfer function is obtained by using the Welch's averaged periodogram method [26]. By the frequency response function of Figure 6 it emerges that with the TV controller, the yaw natural eigen frequency ($f_{G\dot{\psi}\,max}$) is increased by 4 %, thus the an overall faster vehicle response is achieved. On the other hand the yaw dynamic amplification, i.e. the ratio between the maximum magnitude of the yaw-rate response and its steady state value $\left(A_{\dot{\psi}\,max} = \max\left(G_{\dot{\psi}}/G_0\right)\right)$ is slightly deteriorated; thus the controlled vehicle response results more underdamped with respect to the passive vehicle. By comparing the phase delay plot in Figure 6, a faster front end response is seen in the TV controller; thus, the time delay

FIGURE 6 SSI maneuver, dry. Frequency response function between δ_{SW} input and the $\dot{\psi}$ output. Black dashed line = passive vehicle. Blue continuous line = TV sport mode.

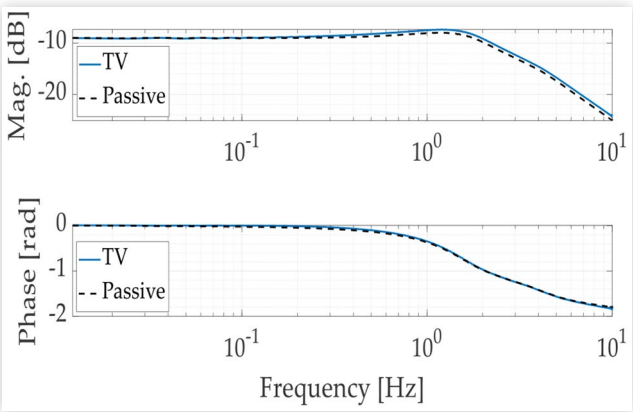

between the steering input and the yaw rate generation observed at 1 Hz, $t_{1,\psi}$, is reduced. Furthermore, the TV improves the rear end response, i.e. the time delay in the lateral acceleration at 1 Hz $t_{1,ay}$. These results are related to the agility of the vehicle. The transitory behavior of the vehicle is unaffected by the steady state tuning modes reported in the SRS maneuver.

The aforementioned performance indicators evaluated through the SRS and the SSI maneuver are summarized in the spider plot reported in Figure 7. The performance are reported in percentage with respect to the baseline passive configuration. The spider plot helps to visualize the overall handling performance of the vehicle. The two LQR tunable modes shape the cornering response improving mainly the sportivity and the stability performances. The feedforward controller contributes to the performance related to the agility of the vehicle.

Processor in the Loop Hardware Implementation

Software-hardware integration for innovative vehicle control systems has gained increasing importance in the overall vehicle development process. The typical V-cycle approach can be used to develop and validate efficient and safe automotive software. To this end, in addition to the MIL simulations carried out in the previous section, the performance of the proposed torque-vectoring control framework is further evaluated with Processor in the loop (PIL) setup [27]. In PIL framework, the controller runs on a dedicated target computer with a compiled application, including all the TV control pipeline; while the vehicle and the driver model runs on the host PC. The driver inputs (steering and brake/throttle command) and the feedbacks from the vehicle are sent via UDP (User Datagram Protocol) to the target computer. At each time step, the controller sends the reference torque signals through the communication network to the host PC. UDP is a packet-based protocol based on Ethernet as physical layer. The Speedgoat Baseline Real Time target machine is used as a rapid control prototyping device to perform PIL.

The software configuration phase for the PIL implementation includes the mapping of all the input/output variables on the target machine and on the host. The target machine and host is connected with UDP communication channels. CarRealTime software provides the real-time solution of the vehicle plant model, thus the Simulink pacing option can be exploited for the synchronization with the controller. The TV controller runs at the set frequency of 100 Hz, while the vehicle plant runs on the host PC at 1 kHz.

The specifications of the Speedgoat Baseline target machine are reported in Table 2. The integration between Speedgoat and Matlab/Simulink enable a rapid prototyping in building and deploying the controller on the target hardware. The simulation results performed under PIL setup will be discussed in the following section. An important metric to check the execution speed of the application is the Average Task Execution Time (TET) [28]. The TV controller algorithm is executed with an average Target Execution Time of 0.3 ms, with a 3 % usage of the available CPU. The TET value represent the average CPU time to execute the proposed code on the target machine. With very slight variations caused by cache, memory access, interrupt latency, and multirate model execution, the average TET is relatively constant [29]. Since the obtained TET is always lower than the sample time of the controller (10 ms), the application is run without any overflow error. Hence, the real time performance of the proposed controller on the considered target machine is demonstrated.

FIGURE 7 Spider – plot of the open loop lateral dynamic performance. Dashed-blue line, passive vehicle. Continuous-orange line, TV sport mode. Continuous-yellow line, TV stability mode. The axe of β_{max} is in logarithmic scale. The parameters are improved towards the external part of the graph.

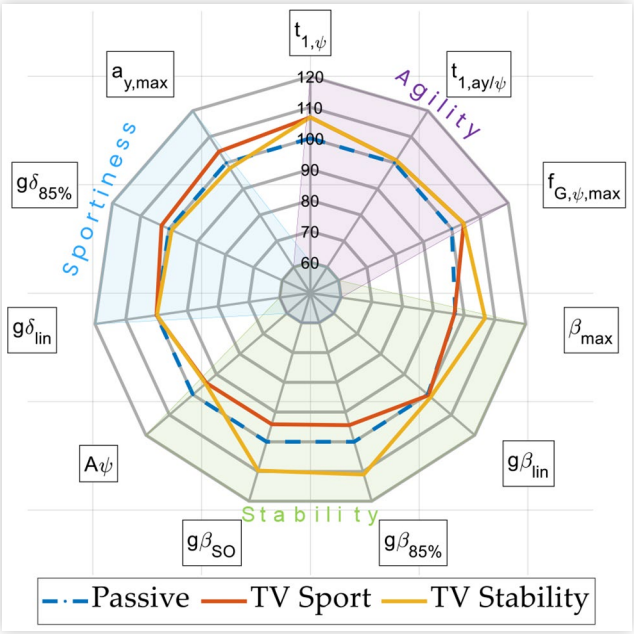

Closed Loop Maneuver

To evaluate the proposed TV control system, a closed loop chicane maneuver is performed. The test has been carried out in the aforementioned PIL set up. The selected simulated scenario is a flying lap track chicane with a radius of 20 m. The host PC includes the vehicle plant model and the driver modeled in Vi Grade Car Real Time. The StaticLapTime event in CarRealTIme is exploited [30]: a quasi static simplified

TABLE 2 Speedgoat baseline real-time target hardware specifications.

CPU	Intel Celeron 2 GHz 4 cores
Memory	4 GB DDR3
Network	1 x USB 3.0, 2 x USB 2.0, Gigabit Ethernet 2
I/O	4 x mPCIe
OS	Simulink Real-Time™
Power	8-36VDC Input Range

FIGURE 8 Closed loop PIL chicane R20 (high adherence) track section. (a) steering wheel angle vs time; dashed-black line, passive vehicle; orange-continuous line, TV sport. (b) Longitudinal speed vs time; dashed-black line, passive vehicle; orange-continuous line, Tv sport. (c) e-motors torque references; blue line, front left; red line, front right; yellow line, rear left; purple line, rear right. (d) corrective yaw moment vs time; blue line LQR contribution; orange line, feedforward contribution.

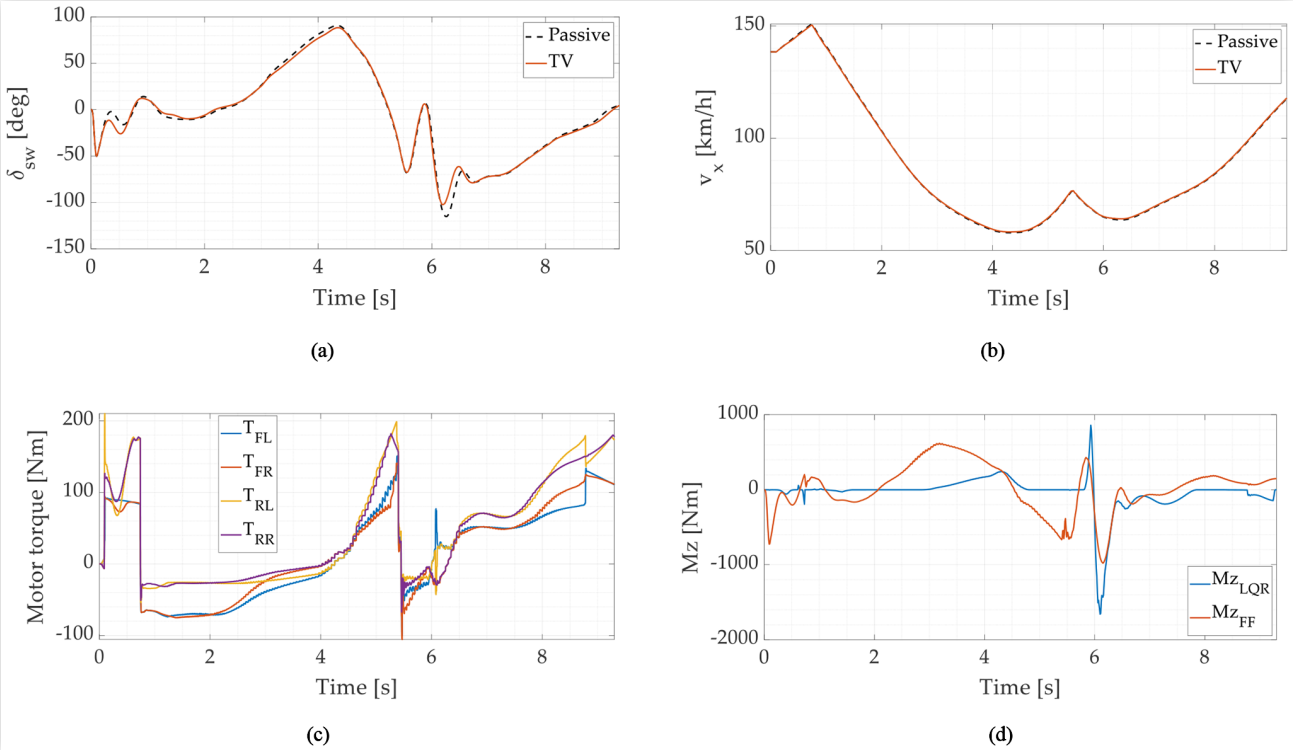

model is used to define a suitable path and velocity profile to minimize the lap time in the selected track section scenario. Then the speed and the path profile are used as reference by the virtual driver in the dynamic vehicle simulation.

The results of the Torque Vectoring PIL simulation in the chicane maneuver are reported in Figure 8 for "Sport" mode (Equation 6).

In Figure 8 (a), it is clear that the TV controller allows the driver to perform the chicane with a reduced steering wheel angle effort, with respect to passive vehicle. The driver is able maneuver around the corners with a higher speed, leading to a reduction of 0.05 s in laptime of chicane. In Figure 8 (c), the torque references provided by the controller running on the target machine are reported. The torque splitting satisfies the system constraints and accomplishes desired outcome producing a suitable profile of yawing moment, as reported in Figure 8 (d). It is worth noting that the feedforward controller's action is predominant in all the instances of maneuver apart from the instant when the vehicle is approaching the limits of stability, where the LQR action is more contributing. The feedforward action is always proactively faster in response to the driver's input with respect to the LQR.

Conclusion

In this work, a novel torque-vectoring control strategy for a four wheel drive electric vehicle was proposed. The controller features the combination of an adaptive Linear Quadratic Regulator with a model based feedforward. The former is designed to shape the steady state cornering behavior of the vehicle according to the desired performance. The feedforward enables a more agile handling behavior of the vehicle in transient conditions. Furthermore the active safety and the stability of the vehicle is guaranteed by the LQR. An optimal torque allocation strategy is presented. It improves the energy efficiency at the vehicle level by reducing the main power losses, leading to overall energy consumption benefits. The energy efficient allocation method is based on the real time solution of a quadratic programming optimization problem with real time constraint.

Simulation results are reported for MIL and PIL set-up. Standard SRS and SSI open loop maneuver have been performed in MIL. Both on high adherence and low adherence conditions, the controller is able to enhance all the key performance indicators of stability, agility and sportivity of the vehicle. The high versatility of the controller is also demonstrated by comparing different tuning modes. The energetic evaluation allow to state the reduction of the main contributions of power losses through the optimum allocation method.

PIL closed loop maneuver are used to evaluate the interaction of the controller in racetrack scenario with a virtual driver. The overall handling performance results are enhanced by the controller action. Furthermore, the PIL allows to evaluate the real-time implementation.

References

1. Vignati, M., Sabbioni, E., and Tarsitano, D., "Torque Vectoring Control for IWM Vehicles," *International Journal of Vehicle Performance* 2, no. 3 (2016): 302-324, doi:10.1504/IJVP.2016.078561.
2. Koehler, S. et al., "Energy-Efficiency Optimization of Torque Vectoring Control for Battery Electric Vehicles," *IEEE Intelligent Transportation Systems Magazine* 9, no. 3 (2017): 59-74, doi:10.1109/MITS.2017.2709799.
3. Mazzilli, V. et al., "Integrated Chassis Control: Classification, Analysis and Future Trends," *Annual Reviews in Control* 51 (2021): 172-205, doi:10.1016/j.arcontrol.2021.01.005.
4. Warth, G., Frey, M., and Gauterin, F., "Design of a Central Feedforward Control of Torque Vectoring and Rear-Wheel Steering to Beneficially Use Tyre Information," *Vehicle System Dynamics* 58, no. 12 (2020): 1789-1822, doi:10.1080/00423114.2019.1647345.
5. Peters, Y. and Stadelmayer, M., "Control Allocation for all Wheel Drive Sports Cars with Rear Wheel Steering," *Automotive and Engine Technology* 4, no. 3 (2019): 111-123, doi:10.1007/s41104-019-00047-9.
6. Rajamani, R., *Vehicle Dynamics and Control* (Springer Science & Business Media, 2011)
7. Kiencke, U. and Nielsen, L., *Automotive Control Systems: For Engine, Driveline, and Vehicle* (2000)
8. Chatzikomis, C. et al., "An Energy-Efficient Torque-Vectoring Algorithm for Electric Vehicles with Multiple Motors," *Mechanical Systems and Signal Processing* 128 (2019): 655-673, doi:10.1016/j.ymssp.2019.03.012.
9. Dalboni, M. et al., "Nonlinear Model Predictive Control for Integrated Energy-Efficient Torque-Vectoring and Anti-Roll Moment Distribution," *IEEE/ASME Transactions on Mechatronics* 26, no. 3 (2021): 1212-1224, doi:10.1109/TMECH.2021.3073476.
10. Parra, A., Zubizarreta, A., and Pérez, J., "An Energy Efficient Intelligent Torque Vectoring Approach Based on Fuzzy Logic Controller and Neural Network Tire Forces Estimator," *Neural Computing and Applications* 33, no. 15 (2021): 9171-9184, doi:10.1007/s00521-020-05680-2.
11. Tang, C. and Khajepour, A., "Wheel Modules with Distributed Controllers: A Multi-Agent Approach to Vehicular Control," *IEEE Transactions on Vehicular Technology* 69, no. 10 (2020): 10879-10888, doi:10.1109/TVT.2020.3019376.
12. Lenzo, B. et al., "Yaw Rate and Sideslip Angle Control through Single Input Single Output Direct Yaw Moment Control," *IEEE Transactions on Control Systems Technology* 29, no. 1 (2020): 124-139, doi:10.1109/TCST.2019.2949539.
13. Novellis, D. et al., "Comparison of Feedback Control Techniques for Torque-Vectoring Control of Fully Electric Vehicles," *IEEE Transactions on Vehicular Technology* 63, no. 8 (2014): 3612-3623, doi:10.1109/TVT.2014.2305475.
14. Liang, Z. et al., "Torque Vectoring and Rear-Wheel-Steering Control for vehicle's Uncertain Slips on Soft and Slope Terrain Using Sliding Mode Algorithm," *IEEE Transactions on Vehicular Technology* 69, no. 4 (2020): 3805-3815, doi:10.1109/TVT.2020.2974107.
15. Pennycott, A. et al., "Sources of Power Loss during Torque–Vectoring for Fully Electric Vehicles," *International Journal of Vehicle Design* 67, no. 2 (2015): 157-177, doi:10.1504/IJVD.2015.068142.
16. Novellis, D., Leonardo, A.S., and Gruber, P., "Optimal Wheel Torque Distribution for a Four-Wheel-Drive Fully Electric Vehicle," *SAE International Journal of Passenger Cars-Mechanical Systems* 6 2013-01-0673 (2013): 128-136, https://doi.org/10.4271/2013-01-0673.
17. Filippis, D. et al., "Energy-Efficient Torque-Vectoring Control of Electric Vehicles with Multiple Drivetrains," *IEEE Transactions on Vehicular Technology* 67, no. 6 (2018): 4702-4715, doi:10.1109/TVT.2018.2808186.
18. Her, H. et al., "Integrated Chassis Control for Optimized Tyre Force Coordination to Enhance the Limit Handling Performance," *Proceedings of the Institution of Mechanical Engineers, Part D: Journal of Automobile Engineering* 230, no. 8 (2016): 1011-1026, doi:10.1177/0954407015597794.
19. Genta, G. and Morello, L., *The Automotive Chassis Volume 2: System Design* (Springer Science & Business Media, 2009)
20. Pacejka, H., *Tyre and Vehicle Dynamics, Ser. Automotive Engineering* (London, U.K: Butterworth-Heinemann, 2006)
21. Boyd, S., Boyd, S.P., and Vandenberghe, L., *Convex Optimization* (Cambridge university press, 2004)
22. Nocedal, J. and Wright, S.J. (Eds), *Numerical Optimization* (New York, NY: Springer New York, 1999)
23. Björck, Å., "Numerical Methods for Least Squares Problems," *Society for Industrial and Applied Mathematics* (1996).
24. ISO 4138. Passenger cars – Steady-state circular driving behaviour – Open-loop test methods. ISO 4138, 2004.
25. ISO 7401. Road vehicles – Lateral transient response test methods – Open loop test methods. ISO 7401, 2011.ù
26. Vold, H., Crowley, J., and Thomas Rocklin, G., "New Ways of Estimating Frequency Response Functions," *Sound & Vibration* 18, no. 11 (1984): 34-38.
27. Tramacere, E. et al., "Processor-in-the-Loop Architecture Design and Experimental Validation for an Autonomous Racing Vehicle," *Applied Sciences* 11, no. 16 (2021): 7225, doi:10.3390/app11167225.
28. Tramacere, E., Castellanos, L.M.M., Amati, N., Tonoli, A. et al., "Adaptive LQR Control for a Rear-Wheel Steering Battery Electric Vehicle," *IEEE Vehicle Power and Propulsion Conference (VPPC)* 2022 (2022): 1-6, doi:10.1109/VPPC55846.2022.10003308.
29. Egel, T., "Real Time Simulation Using Non-causal Physical Models," *SAE International* (2009).
30. Vi-grade, *Vi-CarRealTime 20.3 Documentation* (Vi-grade Gmbh, 2020)

Contact Information

Raffaele Manca
Politecnico di Torino, Corso Duca degli Abruzzi, 24
10129 Torino – ITALY
raffaele.manca@polito.it

Acknowledgments

This work was developed in the framework of the collaboration between Politecnico di Torino and Silk Sports Car Company Srl.

Appendix – Nomenclature

TABLE A1 List of symbols.

Physical symbols, distances, angles and vehicle parameters.	
m	Vehicle mass [kg]
J_z	Yaw moment of inertia [kg m^2]
$l_{F/R}$	Distance of center of gravity from front/rear axle [m]
$tw_{F/R}$	Front/rear trackwidth [m]
h_G	Height of center of gravity [m]
τ	Gear ratio e-motors to wheel
$v_{x/y}$	Longitudinal/lateral velocity [m/s]
$a_{x/y}$	Longitudinal/lateral acceleration [m/s2]
β	Sideslip angle [rad]
ψ	Yaw angle [rad]
$F_{x/y,\,F/R}$	Longitudinal/lateral, front/rear tire forces [N]
M_z	Corrective yaw moment [Nm]
B, C, D	Pacejka tire model: stiffness, shape, peak factor
F_z	Vertical tire load [Nm]
$\alpha_{F/R}$	Front/rear axle sideslip angle [rad]
$\delta_{F/SW}$	Steering angle at front wheel/at steering wheel [rad]
μ	Friction coefficient
K_{US}	Understeering gradient
$T_{i,j}$, $\omega_{i,j}$, $\eta_{i,j}$	Torque [Nm], rotational speed [rad/s], efficiency of the i,j electric machine
R_e	Effective rolling radius [m]
σ	Longitudinal slip ratio
$a_{1...5}$	Electric power estimation coefficient
k_{reg}	Regeneration factor
T_{req}	Required torque for traction [Nm]

Vectors, matrices and variables.	
x, $\mathbf{u}$	State variables vector, input vector
B_u	Input matrix
J_A, J_{BD}, J_{Bu}	State, disturbances and input Jacobian matrices
Q, R, K_{LQR}	Weight, control effort and control action matrices of the linear quadratic regulator
H, $\boldsymbol{f}$	Hessian matrix and linear terms vector of the allocation optimization algorithm
A_{eq}, b_{eq}	Equality constraint state matrix and input vector of the allocation optimization algorithm
$\boldsymbol{A}$, $\boldsymbol{b}$	Inequality constraint state matrix and input vector of the allocation optimization algorithm
Sl_i	Slack variables of the allocation optimization algorithm
$\boldsymbol{lb}$,$\boldsymbol{ub}$	Lower and upper bound vectors of the allocation optimization problem solutions
k_1, k_2, k_3	Tuning parameters of the allocation algorithm

ISSN 0148-7191